PCCP

Accepted Manuscript

ROYAL SOCIETY OF CHEMISTRY

www.rsc.org/pccp

Journal Name

RSCPublishing

ARTICLE

Energetic contributions of residues to the formation of early amyloid-β oligomers

Cite this: DOI: 10.1039/xoxxoooooox

R. Pouplana[a] and J. M. Campanera*[a]

Received ooth January 2012,
Accepted ooth January 2012

DOI: 10.1039/xoxxoooooox

www.rsc.org/

Low-weight amyloid-β (Aβ) oligomers formed at early stages of oligomerization rather than fibril assemblies seem to be the toxic components that drive neurodegeneration in Alzheimer's disease. Unfortunately, detailed knowledge of the structure of these early oligomers at the residue level is not yet available. In this study, we performed all-atom explicit solvent molecular dynamics simulations to examine the oligomerization process of $A\beta_{10-35}$ monomers when forming dimers, trimers, tetramers and octamers, with four independent simulations of a total simulated time of 3 μs for each oligomer system. The decomposition of the stability free energy by MM-GBSA methodology allowed us to unravel the network of energetic interactions that stabilize such oligomers. The contribution of the intermonomeric Van der Waals term is the most significant energy feature of the oligomerization process, consistent with the so-called hydrophobic effect. Furthermore, the decomposition of the stability free energy into residues and residue-pairwise terms revealed that it is mainly apolar interactions between the three specific hydrophobic fragments 31–35 (C-terminal region), 17–20 (central hydrophobic core) and 12–14 (N-terminal region) that are responsible for such a favourable effect. The conformation in which the hydrophobic CTHR-CHC interaction is oriented perpendicularly is particularly important. We propose three other model substructures that favour the oligomerization process and can thus be considered as molecular targets for future inhibitors. Understanding Aβ oligomerization at the residue level could lead to more efficient design of inhibitors of this process.

1. Introduction

The impact of Alzheimer's disease (AD) is increasing year by year due to the ageing of the population in the western world. The underlying cause of the progression of AD is generally assumed to be the oligomerization of soluble amyloid-β (Aβ) peptides.[1,2,3,4,5,6,7] Both *in vitro* and *in vivo* experimental studies on Aβ peptides support the notion that soluble oligomers rather than mature Aβ fibrils are the toxic components that drive neurodegeneration,[8] though there is fierce debate regarding the relationship between auto-assembly and toxicity. Nevertheless, inhibition and/or reversion of the early stages of Aβ oligomerization is currently an attractive therapeutic approach for targeting the progression of the disease.[9]

The proteolysis of the amyloid precursor protein mainly produces 40- and 42-residue peptides. From these initial unstructured monomers, a diverse spectrum of soluble oligomers including dimers, trimers, tetramers[10,11] and other small oligomers up to dodecamers,[12,13,14] or even higher levels of aggregation[15] depending on the experimental conditions are formed,[16] with the monomer form being hundreds of orders of magnitude more concentrated than the oligomers.[17] It remains experimentally unsolved which particular soluble Aβ oligomer is toxic in terms of secondary (low or high β-sheet content), tertiary (parallel or antiparallel) and quaternary (nuclear, fibrillar, compact or globular) structure, although there seems to be a consensus that the low-molecular-weight oligomers are more cytotoxic than higher stoichiometries.[18,19,20,21] Moreover, recent studies suggest that the early oligomeric intermediates may initiate the disease.[6,22,23] The process of aggregation from monomer peptides via soluble oligomers to fibrils is a multistep-nucleated dynamic pathway that is not yet fully understood.[24] Unfortunately, due to the poor solubility of Aβ peptides, the difficulty of forming single crystals and their metastable, transient and highly dynamic character, the main structural features of these soluble oligomers remain unknown, unlike that of the fibrillar structure of Aβ peptides.[25,26]

A plethora of theoretical studies have attempted to reproduce the conditions required for the formation of Aβ oligomers using different strategies. They have provided significant insight into Aβ structures and their possible aggregation mechanism. Pande and collaborators pioneered the use of Markov State Models combined with all-atom molecular dynamics (MD) simulations to reproduce Aβ oligomerization

over long timescales at low concentrations.[27] Jang *et al.* introduced the Replica Exchange Molecular Dynamics (REMD) methodology for the generation of $A\beta_{10-35}$ oligomer ensembles (from monomers to tetramers) in implicit solvent MD simulations, reaching the conclusion that various forms of the dimeric oligomer could exist but that there are limited conformers of the trimeric and tetrameric forms.[28] Similarly, Klim *et al.* used the REMD methodology with an explicit solvent in the case of $A\beta_{10-40}$[29] to ascertain that the aggregation capability is confined to the sequence region 10–23 and the progressive formation of β-sheet structures in higher order oligomers. Unlike previous studies, Xu *et al.* started from fibril structures to generate oligomers but reached similar conclusions about the fact that monomeric $A\beta_{1-40}$ is basically a random coil while oligomers are more fibril-like.[30] P. Derreumaux has extensively modeled and characterized the Aβ aggregation of short peptides using REMD and found that oligomers adopt mainly mixed parallel/antiparallel β-strands but with predominance of antiparallel β-strands.[31,32] Employing a different methodology, Baftizadeh *et al.* characterized the nucleation pathway from disordered aggregates of 18 polyvaline chains to ordered amyloid-like β-structures, reaching the important conclusion that the system first forms a relatively large ordered nucleus of antiparallel β-sheets before a few parallel sheets start appearing.[33] Chong *et al.*[34] employed an alternative methodology to REMD also used by other authors (see methodology section 2.2) consisting of the production of several independent runs of the aggregation process and the subsequent averaging of the independent results to reinforce the hydrophobic collapse as driving force for the oligomerization process.

As revealed above, molecular modeling has dedicated much effort to the simulation of oligomers[16] but the difficulties encountered in the molecular simulation of such a process and the inherent limitation of the present theoretical tools are serious challenges to understanding the oligomerization mechanism at the atomic and residue level.[35] Moreover, almost all analyses have focused exclusively on structural descriptions (secondary and tertiary structures, geometric clustering, etc.) and only a few have attempted some kind of energetic measures. As far as we know, none has attempted a fully consistent energy analysis such as Molecular Mechanics-Generalized Born Surface Area (MM-GBSA) or Molecular Mechanics-Poisson Boltzmann Surface Area (MM-PBSA) using soluble oligomers.[36,37] It is of utmost importance to determine the structural and energetic details of these early oligomers as they could provide insights into the oligomerization process. In the present theoretical work, we focused on the early stages of the oligomerization process since, as mentioned above, some experimental and theoretical works have already pointed to these stages as the origin of toxicity. First, we simulated the spontaneous aggregation of two $A\beta_{10-35}$ units to form the corresponding oligomers (dimers, trimers, tetramers and octamers). To do so, all-atom explicit solvent MD simulations of a minimum duration of 0.6 μs were employed to simulate the self-aggregation process from two units initially separated from each other by a minimum distance of 20 Å in a random conformation. Since a single aggregation process is not representative of such a process we simulated four equivalent systems starting with four random initial relative orientations of both units. The second and main goal was to unravel the network of energetic interactions and their characterization (i.e., polar and apolar) that are present in the oligomers, which may be favoured as the level of aggregation increases. In other words, our main objective was to determine the residue contributions and residue-pairwise interactions that favour the stabilization of early and low-weight Aβ oligomers. To this end, the MM-GBSA methodology enabled the systematic decomposition of the stability free energy into (a) per-residue and residue-pairwise contributions and (b) internal, van der Waals, electrostatic, polar solvation and apolar solvation terms from MD simulations. Finally, the stability free energy matrices were subjected to multivariate data analysis techniques in the search for the crucial residues and residue-pairwise interactions that could drive the initial steps of the aggregation process.

2. Computational methods

2.1. MD simulations of $A\beta_{10-35}$ monomer

The starting point of the present article is the MD simulations performed on the monomer of the $A\beta_{10-35}$ peptide. Two independent MD simulations for a single monomer of $A\beta_{10-35}$ with the amino acid sequence YEVHHQKLVFFAEDVGSNKGAIIGLM were performed in order to obtain an initial structure for simulation of the oligomerization process. The initial conformations of the two $A\beta_{10-35}$ peptides were obtained from two conformations (1 and 9) included in the solid-state NMR structure with PDB code 1HZ3 by Zhang *et al.*,[38] which adopts a collapsed coil structure in water. It is noteworthy that $A\beta_{10-35}$ retains the same structural features,[39,40,41] the crucial central hydrophobic core[42,43] and toxicity[44,45] as the full-length structures $A\beta_{1-40}$ and $A\beta_{1-42}$. This makes this segment a good model for the study of the full-length Aβ peptide.[28,46,47,48,49,50,51,52] The standard protonation state at the physiological pH of 7.4 was assigned to the ionizable residues, as supported by PROPKA calculations.[53] The peptide structures were solvated with TIP3P waters[54] in a periodic octahedral box spanning 12 Å from the peptide structure and neutralized using Na^+ atoms reaching a low and constant ionic concentrations of ≈12 mM for each system.[55,56] The initial monomer system comprised 26 residues, 408 protein atoms and 11164 water molecules (see Table 1 for more details).

Both initial monomeric systems were subjected to minimization, thermalization and production MD simulations of a total duration of 1 μs for each system. A multi-stage protocol was adopted for minimization and thermal equilibration of the systems. Four minimizations (initially with 2000 cycles of steepest descent followed by a maximum of 5000 cycles of conjugate gradient) were run sequentially for

Table 1 Summary of performed simulations.

Oligomer	Monomer	Dimer	Trimer	Tetramer	Octamer
Starting configuration	1HZ3 PDB code	Monomer + monomer	Monomer + dimer	Dimer + dimer	Tetramer + tetramer
Simulated time (number of independent simulations)	1.0 μs (2)	0.6 μs (3) + 1.2 μs (1)	0.6 μs (3) + 1.2 μs (1)	0.6 μs (3) + 1.2 μs (1)	0.6 μs (4)
Total simulated time	2.0 μs	3.0 μs	3.0 μs	3.0 μs	2.4 μs
Number of residues / No. peptide atoms	26 / 408	52 / 816	78 / 1224	104 / 1632	208 / 3264
Number of waters / No. of Na^+ / Na^+ concentration (mM) [a]	3585 / 1 / 12.9	10314 / 2 / 9.3	10552 / 3 / 13.5	13901 / 4 / 13.7	31050 / 8 / 12.5
Total number of atoms [a]	11164	31760	32883	43339	96422

[a] Taken from one of the four (two in the case of monomers) equivalent systems (the number of waters varies slightly among the equivalent systems).

hydrogen atoms, ions, waters and finally all atoms. Thermalization was performed in four steps in which the temperature of the system was increased from 100 to 298 K, each involving 50 ps of MD under the canonical isochoric-isothermic (NVT) ensemble, followed by MD simulation at constant temperature (298 K) and pressure (1 atm) (canonical isothermic-isobaric, NPT) lasting up to 1000 ns. The Amber ff99SB-ILDN force field[57] was used as implemented in AMBER12 package.[58] This new force field exhibits considerably better agreement with the NMR data of proteins, and theoretical studies found that it could be suitable for reproducing the right behaviour of Aβ oligomers.[59] Periodic boundary conditions and Ewald sums (grid spacing of 1Å) were used to treat long-range electrostatic interactions. The non-bonded cut-off distance was maintained at 15 Å and the temperature and pressure were controlled using a Berendsen thermostat and barostat with coupling constant of 0.1 ps. A time step of 2 ps was used, together with the SHAKE algorithm.

2.2. MD simulations of dimers, trimers, tetramers and octamers

The initial structure for the simulation of the oligomerization processes for each oligomer (dimer, trimer, tetramer and octamer) was built from the assembly of two building subunits according to Table 1. This procedure follows the idea that recent experimental studies suggest that Aβ oligomers are formed through the direct interaction of preformed oligomers rather than by subsequent attachment of monomers.[60] Notice that this procedure allows not only the study of the final formed oligomers but also the aggregation process between both subunits. These initial building subunits correspond to the closest structure to the centre of the most populated conformation of each system (monomer, dimer and tetramer) determined by clustering analysis of the C_α RMSD pairwise matrix of snapshots taken at 50 ps intervals in the last 100 ns for all simulations of each mentioned oligomer. In each system, the two subunits were located at a minimum distance of 20 Å between the closest atoms of each subunit, which provides sufficient space for the overall tumbling of each constituent structure. Rather than the replica exchange method, four independent simulations for each system of 0.6 μs duration (thus a minimum of 2.4 μs for each system) with random initial relative orientations of the subunits and different initial velocities were built and subjected to minimization, thermalization and production MD according to the same protocol adopted for monomers. In the case of dimers, trimers and tetramers one of the independent simulations was extended up to 1.2 μs, thus giving a total simulation time of 3.0 μs for these oligomers. Taking into account that structural convergence was already achieved over 0.6 μs in all the simulations (Figure S1), we did not considered necessary to extend them to the octamer case. Notice that the global simulation time reached 13.4 μs (see Table 1 for more details about the simulated systems). Finally, during the last 100 ns of each trajectory (18 independent trajectories), 2000 frames were taken at equally spaced intervals (50 ps) and were subsequently used for the structural analysis and MM-GBSA decomposition of the stability free energy, ΔG. Self-aggregation was observed within the first 100 ns for all systems.

Although we are aware of the simplicity and crudity of the proposed methodology, we expect the average of four converged and long independent MD simulations to give statistically significant results concerning the molecular basis of the initial steps of the oligomerization process of such peptides. As mentioned earlier, a similar procedure was adopted by Matthes *et al.*[61] to study the aggregation of steric zipper peptide segments, by Chong *et al.*[34] to determine the structural heterogeneity of mutants of Aβ peptides or to establish the driving forces of amyloid-β dimerization[62] and by Barz *et al.* to simulate the aggregation of $A\beta_{1-42}$ under experimental concentrations.[63] Likewise, Pannuzo also used independent runs to reveal the early steps of the spontaneous self-assembly of membrane-embedded $A\beta_{1-40}$ peptide;[64] and Pan *et al.* employed three independent runs to study Zn(Aβ) and $Zn(A\beta)_2$ complexes.[65] To sum up, although each simulation of each oligomer gave a different final conformation, the energetic analysis showed common features for the same level of oligomerization and even among different levels of oligomerization (*vide infra*).

2.3. MM-GBSA stability free energy, ΔG

The calculation of the stability free energy (ΔG) of the Aβ peptides was undertaken using the MM-GSA method as implemented in the perl version of AMBER12.[58] The process of aggregation was quantified through the stability free energy of a reaction from a hypothetical averaged monomer of all dimers to the corresponding oligomer. Therefore, to make the energies comparable among the different oligomers they were referenced to the mentioned averaged free energy of both monomers of dimers and corrected by the number of monomers as follows

$$(1)\quad \Delta G=\frac{G_{complex}-k\cdot G_{average,monomer}}{k}$$

where ΔG is the stability free energy, $G_{complex}$ is the free energy of the complex, $G_{average,monomer}$ is the average free energy of both monomers that form the dimers and k is the number of monomers in the oligomer complex. Thus, ΔG is actually a relative stability free energy in this work.

The total stability free energy (ΔG_{total}) is obtained by the averaged stability free energy of the involved molecules of an ensemble of MD snapshots. The MM-GBSA stability free energy (G) is calculated by combining the molecular mechanical energies with the continuum solvent approaches, which, after applying equation 1, can be expressed as follows

$$(2)\ \Delta G_{total} = \Delta E_{MM} + \Delta G_{sol} = \Delta E_{int} + \Delta E_{ele} + \Delta E_{vdW} + \Delta G_{sol,pol} + \Delta G_{sol,apol}$$

where ΔE_{MM} is the molecular mechanics energy expressed as the sum of the internal energy (bonds, angles and dihedrals) (ΔE_{int}), electrostatic energy (ΔE_{ele}), van der Waals term (ΔE_{vdW}) and ΔG_{sol} accounts for the solvation energy that can be divided into the polar and nonpolar part ($\Delta G_{sol,pol}$ + $\Delta G_{sol,apol}$). Additionally, ΔG_{total} and any of the other terms can be decomposed into ΔG^{intra} and ΔG^{inter}, where the former accounts only for the stability free energy change related to the intramonomeric interactions compared to those present in the average energy profile of the monomers of the dimers taken as a reference, and the latter for the intermonomeric interactions exclusively. This type of decomposition was employed by the authors to describe the binding free energy between two $A\beta_{10-35}$ monomers to form a dimer.[66]

2.4. Per-residue and residue-pairwise decomposition of the MM-GBSA stability free energy

Since we were mainly interested in describing the network of energy interactions at the different levels of aggregation, all energy terms of equation (2) were decomposed into per-residue and also residue-pairwise contributions according to the standard MM-GBSA scheme:

$$(3)\quad \Delta G=\sum_{i=1}^{n}\Delta G_i=\sum_{i=1}^{n}\sum_{j=1,j\le i}^{n}\Delta G_{i,j}$$

where n is the total number of residues, ΔG_i are the per-residue contributions and $\Delta G_{i,j}$ are the residue-pairwise interaction contributions. Notice that only ΔE_{ele} and ΔE_{vdW} are strictly residue-pairwise decomposable whereas the solvation terms are not consistently decomposable since the effective radii for GB are dependent on the surroundings.[37,67] Consequently, only the former terms were used in the residue-pairwise decomposition. Moreover, the stability free energy as expressed in equation (2) does not account for the entropic term of the molecular mechanics part (ΔE_{MM}), unlike the solvation part (ΔG_{sol}). The configurational entropy, which corresponds to the entropy of the ΔE_{MM} part, cannot be decomposed into per-residue and residue-pairwise components and consequently was not included in the values of the final stability free energies. Thus, calculations were not used to evaluate the spontaneity of the aggregation process due to the lack of this term, but the residue interaction network as the level of aggregation increased. This methodology has previously been used by the authors to elucidate the signal transmission mechanism in the allosteric regulation of protein kinases C.[68] Likewise Berhanu and Masunov employed MM-GBSA per-residue decomposition (but not residue-pairwise decomposition) to study preformed short β-sheet amyloid fibrils.[69,70]

The fragmental decomposition yielded a high number of components. For instance, ΔE_{vdW} in the dimer can be split into 52 residue-based terms and 1378 ([52 · 52 + 52]/2) distinctive residue-pairwise interactions. As the number of monomers increased, the residue-pairwise interactions also reached high numbers, but to circumvent this difficulty, the average energetic profile of the 26 distinct residues per monomer was used instead of the specific energy profile of all residues in the whole oligomer. In this way, the per-residue energy matrices comprised 26 contributions regardless of the level of aggregation and the residue-pairwise energy matrices comprised only 351 ([26 · 26 + 26]/2) distinct contributions instead of the unaffordable 21,736 ([208 · 208 + 208]/2) interactions in the octamer, for instance.

All final free energy terms, either total or fragment-based, were calculated on the basis of averaged values over 8000 frames (4 x 2000) sampled during the last 400 ns (4 x 100 ns) using the four independent trajectories for each oligomer. To do so, the MM-GBSA source data was converted into energy matrices of the form of frames as rows and energy contributions as columns (frames *x* energy contributions) using a perl script developed in-house. For each of the oligomers, we compiled a total energy matrix (non-decomposed matrix) with 8000 rows and the six energy terms of equation 2 as columns (ΔG_{total}, ΔE_{int}, ΔE_{ele}, ΔE_{vdW}, $\Delta G_{sol,pol}$ and $\Delta G_{sol,apol}$), along with six residue matrices (8000 x 26) and six additional residue-pairwise-based energy matrices (8000 x 351) for each of the six terms of equation 2. This perl script will be provided by the authors upon request.

2.5. Multivariate data analysis of the energy matrices

To analyse this large amount of data, we used a step-by-step procedure in which we analysed first the non-decomposed matrices, second the residue-based matrices and finally the voluminous residue-pairwise matrices. This procedure allowed a focused search of the residue-pairwise matrices since information about the most important terms and residues had been gathered previously. Apart from the average analysis

performed over 8000 frames (400 ns) for each oligomer, which could be considered as a static analysis, a dynamic or correlation analysis was also accomplished over the energy matrices in the search for correlated energy contributions that could unravel the aggregation mechanism. Such analysis may, with effort, identify correlated energetic changes at total, residue and residue-pairwise energy contributions, and thus, highlight similarities and differences between dimers, trimers, tetramers and octamers. In this regard, the partial least squares (PLS) regression technique provided suitable multivariate strength to accomplish our aim to discover important energy terms in the voluminous energy matrices. To the best of our knowledge, this is the first attempt to apply multivariate data analysis to the total and decomposed energy matrices derived from MM-GBSA calculations. When necessary, a t-test with a p-value of 0.01 was performed to assess the differences between two variable distributions. The R program was used for all statistical analyses and graphics.[71]

2.6. Structural analysis

The trajectories were analysed using Bio3d package of R.[72] The DSSP algorithm was used to assign secondary structures and hydrogen bond presence.[73] To determine the hydrogen-bond formation between two residues a threshold of -1 kcal/mol was applied to the DSSP output, which evaluates the presence of a hydrogen bond by calculating the bond energy between all possible acceptors and donors within a certain distance. The interaction between two intermonomeric hydrophobic strands was evaluated structurally by the distance between the centre of mass of C_α atoms of both subunits; we considered that both strands interact when the average distance is kept below 10 Å. Additionally, the angle formed between the average subunit vectors that connect the C_α atoms from C-terminal to N-terminal of each subunit was computed for all interacting strands. This angle lies between 0° and 180° and if higher than 135° an antiparallel orientation between both interacting strands is considered; when the angle is lower than 45° a parallel orientation is recorded, and between 45° and 135° a perpendicular orientation is assigned.

3. Results and Discussion

3.1. Convergence analysis

The first 100 ns of each simulation corresponding to the thermalization and first production time (where assembly occurs between both units) were eliminated for the convergence analysis. Convergence of the 18 simulations was assessed by the time evolution of the root mean square deviation (RMSD) of the backbone heavy atoms (see Figure S1), radius of gyration (Figure S2) and secondary structure (Figure S3, S4, S5, S6 and

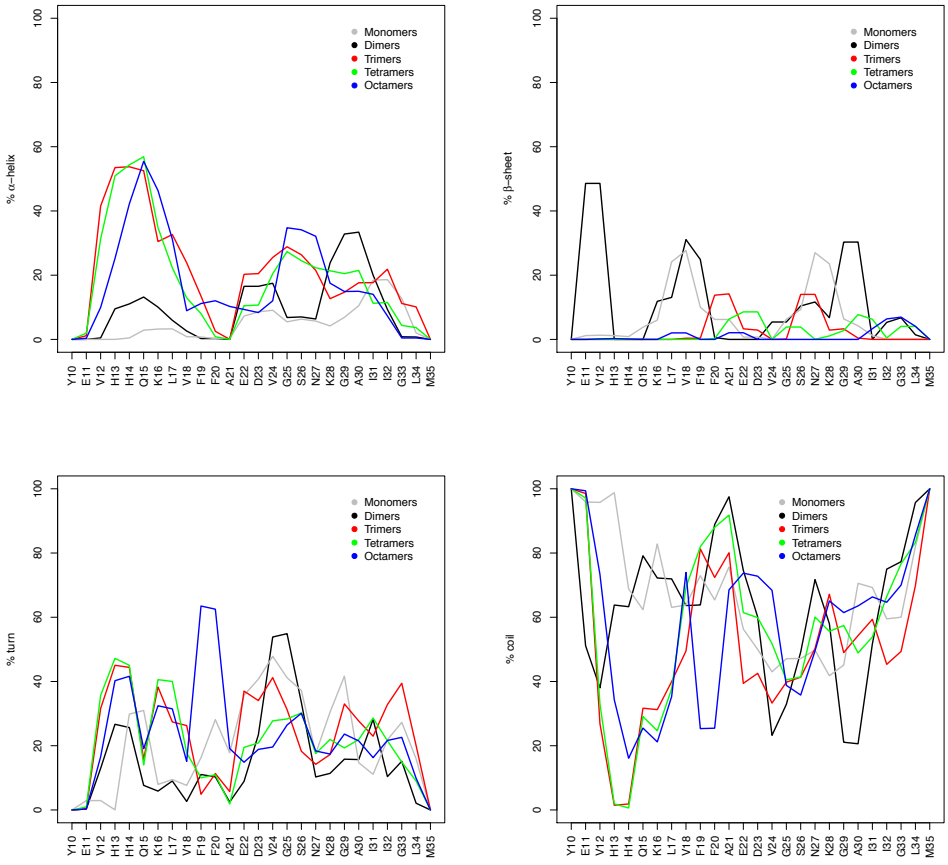

Figure 1 Proportion of the secondary structure elements (α-helix, β-sheet, turn and coil) per residue in each oligomer.

S7) and several other magnitudes that will be presented throughout the article. These figures illustrate that after a reorganization period all oligomer structures reach structural stability. Therefore it is reasonable that the first contacts of both subunits show high structural variability, and that episodes of disaggregation and subsequent aggregation occur until the aggregate is fully formed, which happens before 400 ns in all systems. The evolution of the secondary structure (computed using the DSSP program[73]) is also commonly used as a measure of convergence of MD simulations. However small changes were observed during the last 0.5 μs of each simulation (Figure S3, S4, S5, S6 and S7), which means that the initial steps of oligomerization are related to reorganizations in the tertiary and quaternary structure, as found by Barz *et al.*[63] These results confirm that the in-depth analysis of the MM-GBSA decomposition can be undertaken for the purposes of the paper during the last 100 ns of each simulation, during which structural stability is achieved.

3.2. Secondary and tertiary structure

The analysis of the secondary and tertiary structure has become a validation tool for theoretical studies. According to literature, monomers contain the highest amount of α-helix and oligomers contain an increasing proportion of β-sheet as the order of aggregation increases, although turn and coil structures are dominant overall. In the oligomers simulated here, averaged over all conformations and residues, the secondary structure is mostly an unstructured coil (67%, 66%, 62%, 46% and 58% for monomers, dimers, trimers, tetramers, and octamers, respectively) and turn (20%, 18%, 19%, 32% and 23%), with a substantial percentage of α-helix (5%, 9%, 17%, 19% and 17%) and a small but significant presence of the β-sheet conformation (6%, 7%, 2%, 3% and 2% respectively, see Table S1 for the corresponding standard deviations). Notice that there is little change in the overall secondary structure of oligomers compared to that found in monomers. On the other hand, the relatively low presence of β-sheets is consistent with the 4.8% and 5.6% for $A\beta_{40}$ and $A\beta_{42}$ dimers respectively found by Barz and Urbanc,[74] the 9% for the $A\beta_{42}$ monomer found by Chong *et al.*[34] in their computational studies and the characterization of the low-order oligomers studied experimentally by Ahmed *et al.*[75] Moreover the low β-sheet content could indicate that the oligomerization process simulated here is indeed in its initial stages and that this early aggregation somehow precedes β-sheet formation.

Regarding the residue propensities, there appears to be a high propensity (>50%) for an α-helix in the 11–17 amino acid residues region, whereas the turn is more common in the central region of the monomer (residues 19–25) although this varies among oligomers, see Figure 1. Although very small percentages of β sheet structures were found, the highest percentage was located in the C-terminal region (residues 26–34), except in dimer oligomers in which they also populate the N-terminal region. On the other hand, the terminal tails, amino acid residues 34–35 and 10–11, are mostly random coils. As reported in previous experiments, only some Aβ regions (especially N-terminal region) show a high propensity to form α-helix,[76] meanwhile the C-terminal region of Aβ specifically adopts a β-sheet conformation[77,78,79,80] in line with the present work, even though our study considers a shorter C-terminal fragment. Therefore, the secondary structure remains almost invariant during the initial stages of the oligomerization process and consequently side-chain structure is foreseen to play the major role in interstrand interactions in this initial process.

Table 2 Number of hydrogen bonds per monomer classified into intermonomeric and intramonomeric contacts.[a]

	Monomers	Dimers	Trimers	Tetramers	Octamers
Inter		1.5±0.4	0.9±0.2	0.7±0.3	1.4±0.2
Intra	5.4±1.5	5.6±0.8	6.5±0.6	5.7±0.7	3.9±0.4

[a] Hydrogen bonds were detected using DSSP program as implemented in Bio3d package of R.

A hairpin (or U-turn or strand-turn-strand conformation) formed by $V^{24}GSN^{27}$ residues is the most common tertiary structure adopted by monomers within oligomers. Several theoretical papers indicate that the maintenance of the intramonomeric interaction between K28 and D23 is largely responsible for this conformation.[81-82] Indeed, our structural analysis revealed that K28-D23 is the most common intramonomeric interaction among all interactions separated by a minimum of four residues[83] in all oligomers and is present in 13%, 8%, 14% and 28% of all monomers of dimers, trimers, tetramers and octamers, respectively, which compares well with the 15% presence of this interaction in monomers. The prominent role of the K28-D23 contact is also highlighted in Table S2 since its associated intramonomeric electrostatic energy is the strongest among all intramonomeric interactions. The second most important intramonomeric interaction appeared to be between E22 and K16, although it is very uncommon except for monomers of trimer oligomers (30%).

Analysis of the intra- and intermonomeric hydrogen bonds (Table 2) confirmed our view of the preservation of the main features of the monomer in the structures of oligomers that had already emerged from the secondary and tertiary analysis. On average, there are up to five times more hydrogen bonds in the intramonomeric network than in the intermonomeric one in all oligomers, with 5.4 compared to 1.1 hydrogen bonds per monomer on average. This does not seem to change as the level of aggregation increases although the octamer oligomer has the lowest content of intramonomeric hydrogen bonds. Moreover, analysis of the specific hydrogen bonds revealed that intermonomeric contacts are not conserved among oligomers or different simulations of the same oligomer, in contrast to the situation in the intramonomeric network, in which it was possible to identify the most common contacts easily (mainly hydrogen bonds of the α-helix in the N-terminal region, residues 11–17). These results suggested that hydrogen bonds do not play a crucial role in the early stages of oligomerization, which is consistent with other works.[62]

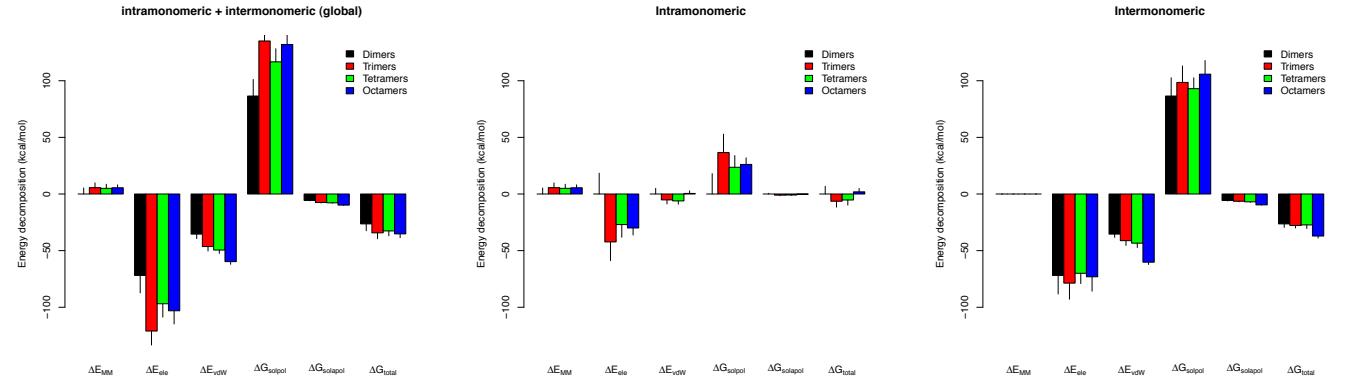

Figure 2 Decomposition of the stability free energy (ΔG_{total}) and its constituent terms into intramonomeric and intermonomeric contributions, in kcal/mol. Mean values and standard deviation values are represented. See also Table S3 for the numeric version.

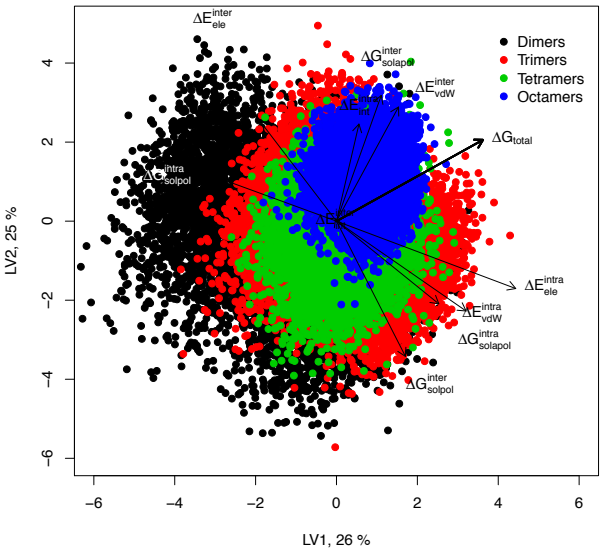

Figure 3 PLS biplot of the decomposition of the total stability free energy (ΔG_{total}) into its constituent terms splitted by intra and inter contributions. LV stands for latent variable. Dots represent MD frames, solid lines correspond to the energy terms (*x* variables) and the bold line the predicted variable (*y* variable) in the PLS model. The percentage of the explained variability of the *x* variables for each latent variable is also displayed in the corresponding axis. Notice the opposite behavior of the intermonomeric $\Delta G_{sol,pol}$ in comparison to the intermonomeric ΔE_{ele}, in other words higher electrostatic contribution to stability free energy is only achieved in contraposition to lower polar solvation contributions. This energetic behavior is common for proteins and peptides that balance solvation and internal stability.[109] Two final important things to remark, first, the arrow of the total stability free energy (ΔG_{total}) displays the direction of its highest variability, which points in the direction that permits the visual separation of the level of aggregation from dimers to octamers. And second, the compactness of the oligomer clusters in the biplot could also be a measure of the convergence of the present results.

Finally it was worth paying attention to the quaternary structure of oligomers by analysing the radius of gyration, which is a measure of the degree of compactness. This magnitude varies, on average, from 9.3 ± 1.2 Å in monomers, 10.6 ± 0.7 Å in dimers, 12.6 ± 0.8 Å in trimers, 15.3 ± 1.4 Å in tetramers to 19.4 ± 1.5 Å in octamers, being similar to that of globular proteins and intrinsically disordered proteins with the same number of residues.[84]

3.3. The increase in intermonomeric vdW interactions in the oligomerization process: the "hydrophobic collapse"

After briefly analysing the main structural elements of the oligomer ensembles we now shift to the MM-GBSA analysis, which is the main purpose of the present article. Figure 2 plots (and Table S3 lists) the decomposition of the total averaged stability free energy for dimers, trimers, tetramers and octamers for the last 100 ns of the four independent simulations of each oligomer. The stability free energy in all simulated systems is dominated by the apolar terms over the polar ones, for instance in dimers ΔG_{apolar} is computed to be -41.1 kcal/mol (ΔE_{vdW}=-35.4 kcal/mol + $\Delta G_{sol,apol}$=-5.7 kcal/mol) whereas the ΔG_{polar} yields the unfavourable contribution of +14.6 kcal/mol (ΔE_{ele}=-71.9 kcal/mol + $\Delta G_{sol,pol}$=86.5 kcal/mol). Octamer and trimer oligomers contain the highest stability free energy (-35.2 and -34.3 kcal/mol per monomer respectively) followed by tetramer (-32.6 kcal/mol) and dimer (-26.4 kcal/mol) oligomers. With the exception of trimers and octamers, a t-test revealed statistically significant differences. Thus, the weak rise in the stability free energy as the level of aggregation increases could be a sign of the propensity of the aggregation process. Moreover, the energy decomposition identified the vdW term as the unique source of the intrinsic stability of oligomers and also for the increase in the stability free energy from dimers to octamers, with 24.3 kcal/mol of increase from -35.4 kcal/mol in dimers to -59.7 kcal/mol in octamers representing a 69% increment. The other terms either did not suffer substantial variations (ΔE_{int}, $\Delta G_{sol,apol}$) or did not show any clear trend (ΔE_{ele} and $\Delta G_{sol,pol}$).

However, the previous decomposition does not indicate whether the stable vdW interaction originates in the intramomeric network or alternatively in the intermonomeric one. Analysis of the intra/inter decomposition revealed not only that the intermonomeric total stability free energies is favourable and increases steadily (and statistically significant) from dimers, trimers and tetramers to octamers (-26.4, -27.8, -27.3 and -37.1 kcal/mol respectively) whereas the intramonomeric interaction energies show erratic behaviour (0.0, -6.4, -5.3, 1.9 kcal/mol), but also that the intermonomeric vdW stability free energies are responsible for such stability (-35.4, -41.2, -43.4 and -60.2 kcal/mol; all differences being statistically significant; see Figure 2 or Table S3). The combination of the two phenomena gives rise to a hydrophobic effect that as far as we know has not previously been quantified in such long amyloid oligomers. This hydrophobic effect refers to the first mechanistic events of the oligomerization process prior to fibril formation and is based on the notion that the major driving force for the oligomerization of Aβ is the hydrophobic role played mainly by the C-terminal hydrophobic region (31–42 residue region).[85] According to Cheon *et al.* [86] and Hwang *et al.*,[87] these results suggest again that we were analysing the first step in the oligomerization process, which is characterized by a hydrophobic coalescence, whereas in the second step of the oligomerization oligomers would undergo a reorganization driven by intermonomeric hydrogen bond formation which, indeed, was not envisaged in the present MD simulations. Our findings agree also with the fact that MD simulations demonstrate that after a nucleation stage an accommodation stage governed by internal vdW forces takes place in $A\beta_{42}$ dimerization.[62] Another point to note from Figure 2 and Table S3 is that the standard deviation of all terms decreases significantly from dimers to octamers indicating that the aggregation process rigidifies the overall structures. To summarize we present Figure 3, which captures all these interrelationships visually in a PLS biplot with the energy profile of dimers, trimers, tetramers and octamers clearly differentiated by the intermonomeric vdW and apolar solvation terms.

3.4. The importance of 12–14 (NTHR), 17–20 (CHC) and 31–35 (CTHR) amino acid residues in the hydrophobic collapse

Having determined that the intermonomeric vdW interactions are responsible for the stability of all oligomers, we turned our attention to the most relevant residues involved in this effect. In order to do so, the intermonomeric vdW term was decomposed further into residue terms for all oligomers (see Figure 4, Table S4 and S5). According to the decomposition, all residues contribute to the vdW stabilization without exception, although three regions contain contributions lower than -2.3 kcal/mol per residue in octamers: on one side of the U-turn a) Y10, H13, H14, which with the inclusion of E11 and V12 becomes the N-terminal hydrophobic region (NTHR), b) L17, F19 and F20, which with the inclusion of V18 coincides with the central hydrophobic core (CHC), and on the other side of the U-turn c) I31, I32, L34 and M35, which hereafter with the inclusion of G33 will be called the C-terminal hydrophobic region (CTHR). In addition, the intermonomeric total stability free energy decomposed into residue contributions (Figure 5, Table S6 and S7) confirmed the dominance of the vdW term and also the favourable role in the oligomerization of these specific residues, with the exception of Y10 and E11 of the NTH region, which despite the stabilizing vdW effect yield destabilizing positive values when taking into account the polar

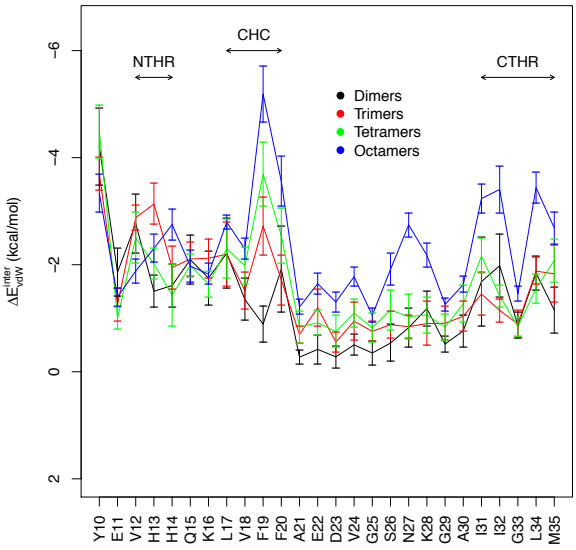

Figure 4 Per-residue decomposition of the intermonomeric vdW stability free energy, ΔE_{vdW}^{inter}, in kcal/mol. Three fragments emerge as the most relevant to the ΔE_{vdW}^{inter}, CTHR=$I^{31}IGLM^{35}$; CHC=$L^{17}VFF^{20}$ and NTHR=$V^{12}HH^{14}$.

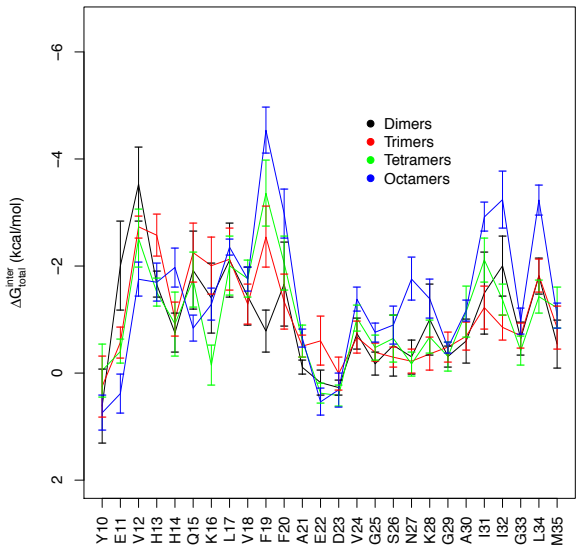

Figure 5 Residue decomposition of the intermonomeric total stability free energy, ΔE_{total}^{inter}, in kcal/mol. Four residues contribute negatively to the stability: Y10, E11, E22 and D23.

Table 3 Contributions and their relative weight of the three hydrophobic fragments (CHC, CTHR and NTHR) to the intermonomeric vdW stability energy, ΔE_{vdW}^{inter}, in kcal/mol.[a]

Mean±sd (%)	Dimers	Trimers	Tetramers	Octamers
CTHR	-7.5±3.0 (21)	-7.2±2.5 (18)	-8.1±1.6 (19)	-14.2±1.8 (24)
CHC	-6.4±3.6 (18)	-8.1±2.9 (20)	-10.5±3.1 (24)	-13.8±1.9 (23)
NTHR	-5.9±1.5 (17)	-8.0±1.5 (19)	-6.0±1.1 (14)	-6.9±0.8 (12)
Hydrophobic Fragments	-19.8±2.8 (56)	-23.3±4.6 (57)	-24.5±4.4 (57)	-35.0±3.4 (59)
Total	-35.4±5.9 (100)	-41.2±8.6 (100)	-43.4±7.8 (100)	-60.2±4.1 (100)

[a] CTHR=$I^{31}IGLM^{35}$; CHC=$L^{17}VFF^{20}$ and NTHR=$V^{12}HH^{14}$.

part. Therefore both residues were excluded from the NTH region, which hereafter only contains $V^{12}HH^{14}$. Finally, Table 3 summarizes the main statistics of the importance of these fragments in comparison to the total intermonomeric vdW stability energy. These fragments give rise to almost 60% of the intermonomeric vdW stability though they represent only 46% of the total number of residues. Moreover, two of them, CTHR and CHC, excel in their hydrophobic contribution to the stability free energy.

Below, some of these residue contributions are discussed according to the values presented in Figure 4 and Table S4. For instance, the impact of H14 (NTHR) on intermonomeric vdW stability increases from -1.6 kcal/mol (dimers), -1.9 kcal/mol (trimers) and -1.4 kcal/mol (tetramers) to -2.8 kcal/mol (octamers) in the same manner as the contribution of F20 (CHC), from -1.9, -1.7, -2.5 to -3.6 kcal/mol respectively, and L34 (CTHR), from -1.8, -1.9, -1.6 to -3.4 kcal/mol respectively. In all three cases, statistically significant differences were found between the octamer energetic profile and that found in dimers, trimers and tetramers. Note in Figure 4 and Table S4 that not only were these residues those that contributed most to the vdW stability within each oligomer (especially in CTHR and CHC), but also that these residues were those that varied most among oligomers. A step towards establishing the role of the identified residues would be to reveal their dynamic relationship with the intermonomeric vdW stability energy, in other words the correlation of these residue contributions with this magnitude. To this end, the multivariate PLS regression technique (see Figure S8) was used to extract the relevant trends between the intermonomeric vdW energy and the vdW per-residue contributions reaching similar conclusions to what has been explained previously.

Numerous articles have highlighted the importance of these residues in the oligomerization process. First, the crucial role of H13 and H14 in the oligomerization process in the presence of Cu(II) and Zn(II) has already been reported.[88,89] Second, the importance of the aromatic rings of F19 and F20, especially the former, for aggregation has also already been pointed out experimentally by Gazit and collaborators[90,91] and others.[92] This finding compares well with the fact that five small-molecule drugs interacted preferentially with the side chains of F19 and F20 in a reported docking study and thus interfered in the aggregation process.[93] Third, the unfavourable role of Y10 and E11 of the N-terminal fragment in the aggregation could reflect the results of experimental[94] and theoretical[95] studies that indicate that N-terminal truncated oligomers increase the propensity for oligomerization. Nevertheless, our results suggest that only polar residues (Y10 and E11), unlike apolar residues, in NTHR are responsible for such a negative effect. Fourth, the prominent role of the CTHR fragment is consistent with the fact that Frandinger *et al.* and Wu *et al.* reported that C-terminal fragments (CTFs) of $A\beta_{42}$ may inhibit Aβ oligomerization by disrupting important interactions.[96,97] Similarly, cysteine scanning mutagenesis revealed that replacements of any six hydrophobic residues in the segments 31–34 disrupted hexamer and tetramer formation.[98] Finally, several other studies have also reported that the C-terminal region plays a dominant role in $A\beta_{1-40}$ oligomer formation.[99,100]

Table 4 The 15th most favourable intermomeric vdW stability free energies (ΔE_{vdW}^{inter}) of selected residue-pairwise interactions, in kcal/mol.[a,b]

	Dimers	Trimers	Tetramers	Octa.	Type [c]
F19-L17	-0.1	-0.1	-0.5*	-1.0*	CHC-CHC
F19-V18	0.0	-0.2	-0.4*	-0.7*	CHC-CHC
I31-H14	-0.5*	-0.2	-0.4*	-0.6	CTHR-NTHR
K28-F19	-0.1	0.0	-0.2	-0.6	-
N27-F19	0.0	0.0	-0.3*	-0.6	-
I32-F19	-0.1	-0.3	-0.4	-0.6	CTHR-CHC
I31-L17	-0.2	-0.5*	-0.5*	-0.6	CTHR-CHC
I31-V18	-0.1	-0.1	-0.3	-0.5	CTHR-CHC
F20-Y10	-0.2	-0.5*	-0.8*	-0.5*	-
L34-I32	-0.2	-0.1	-0.1	-0.5*	CTHR-CTHR
M35-H14	-0.1	-0.3*	-0.1	-0.5	CTHR-NTHR
K28-F20	-0.5*	-0.1	-0.1	-0.5	-
L34-Y10	-0.2*	-0.3*	-0.4*	-0.5	-
I31-F19	-0.1	-0.2*	-0.4*	-0.5	CTHR-CHC
L34-F19	-0.3*	-0.1	-0.2	-0.4	CTHR-CHC

[a] Standard deviation lower than 0.2 kcal/mol in all cases except those with * that yield values between 0.2 and 0.6. [b] Ranked according to the octamers energies. [c] CTHR=$I^{31}IGLM^{35}$; CHC=$L^{17}VFF^{20}$ and NTHR=$V^{12}HH^{14}$

3.5. The directionality of the NTHC, CHC and CTHR interactions.

To gain further insight regarding the role of the abovementioned fragments, the ten strongest intermonomeric vdW stability energies of residue-pairwise interactions were compiled in Table 4. Residue-pairwise analysis allowed us to determine their relative strength. Basically, significant contributions between all three hydrophobic fragments are found in all directions. At this level of decomposition, the

Table 5 Intermonomeric vdW stability free energies (ΔE_{vdW}^{inter}) between the three identified hydrophobic regions CTHR, CHC and NTHR, in kcal/mol.[a]

	Dimers	Trimers	Tetramers	Octamers	Global[b]
CTHR-CHC	-4.8±2.8	-3.3±3.2	-5.0±2.1	-6.6±1.0	-4.9±2.7
CTHR-NTHR	-2.9±3.2	-2.3±1.2	-1.8±1.0	-4.7±1.2	-2.9±2.7
CHC-CHC	-1.2±1.4	-1.8±1.8	-2.6±1.5	-3.4±1.3	-2.3±1.5
CHC-NTHR	-0.9±0.6	-2.6±1.8	-3.2±1.5	-2.0±0.5	-2-2±1.7
CTHR-CTHR	-0.6±0.8	-1.2±1.0	-0.6±0.5	-3.6±1.4	-1.5±1.6
NTHR-NTHR	-0.7±0.8	-1.7±0.9	-0.5±0.3	-0.3± 0.2	-0.8±0.8

[a] CTHR=$I^{31}IGLM^{35}$; CHC=$L^{17}VFF^{20}$ and NTHR=$V^{12}HH^{14}$; [b] Ranked according to the averaged interaction among all oligomers.

pairwise energy profile of all oligomers is similar and with the exception of some specific interactions the differences between oligomers are not significant. Nevertheless, F19-L17 (CHC-CHC) varies, on average, from nonexistent interaction in dimers to -0.1 kcal/mol in trimers, -0.5 kcal/mol in tetramers and -1.0 kcal/mol in octamers; I31-H14 (CTHR-NTHR) from -0.5 kcal/mol to -0.2, -0.4 and -0.6 kcal/mol; L34-F19 (CTHR-CHC) from -0.3 to -0.1, -0.2 and -0.4 kcal/mol; and I31-F19 from -0.1 to -0.5. Moreover, this interaction was identified as a favourable contact in other studies. [75,101,102]

Table 5 reveals the relative strength of all possible hydrophobic interactions between the considered fragments. All interactions between the three-abovementioned hydrophobic fragments (NTHR, CHC and CTHR) were computed and characterized according to their intermonomeric vdW stability energy. First, at this level of detail there are no significant differences among oligomers, which suggest that the oligomerization mechanism is fairly similar in each one. Second, one interaction emerges as the most favourable, CTHR-CHC (on average -4.9 kcal/mol in vdW stability energy), followed by three intermediate interactions CTHR-NTHR (-2.9 kcal/mol), CHC-CHC (-2.3 kcal/mol) and CHC-NTHR (-2.2 kcal/mol), all of them especially relevant in octamer oligomers. Notice that there are higher numbers of possible contacts between two different hydrophobic regions than between the same regions. So, for instance, in a dimer oligomer there are two possible CTHR-CHC hydrophobic interactions ($CTHR_1$-CHC_2 and CHC_1-$CTHR_2$) but only one CHC-CHC interaction (CHC_1-CHC_2). This must influence their relative importance in favour of interactions between different hydrophobic regions rather than between the same regions.

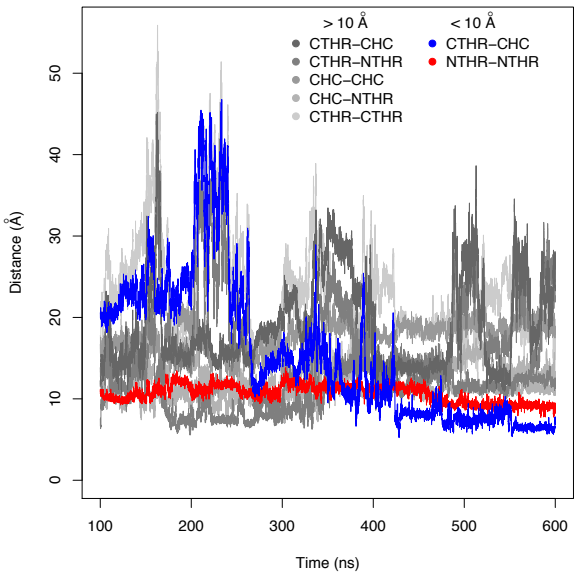

Figure 6 All possible distances among the C_α mass centre of the three hydrophobic fragments (CTHR, CHC and NTHR) are tracked along one of the simulations of the dimer. As observed, one of the CTHR-CHC contacts (blue) and the NTHR-NTHR contact (red) get stabilised and converged below 10 Å at the end of the simulation.

In light of the importance of these hydrophobic contacts we counted and characterized all types of hydrophobic interactions present in our simulations in Table 6 (see also structural

Table 6 Total number of intermonomeric hydrophobic contacts between CTHR, CHC and NTHR hydrophobic fragments and their characterisation into perpendicular, parallel and antiparallel orientation of the interacting strands in the four independent simulations for each oligomer.[a]

Total (Perpendicular/Antiparallel/Parallel)	Dimers	Trimers	Tetramers	Octamers	Total number per type
CTHR-CHC	2 (2/0/0)	2 (2/0/0)	4 (2/1/1)	12 (8/2/2)	20 (14/3/3)
CTHR-NTHR	2 (0/2/0)	2 (2/0/0)	3 (3/0/0)	9 (6/1/2)	16 (11/3/2)
CHC-CHC	0	1 (0/0/1)	2 (2/0/0)	7 (4/2/1)	10 (6/2/2)
CHC-NTHR	0	1(0/0/1)	3 (2/0/1)	6 (3/1/2)	10 (5/1/4
CTHR-CTHR	0	0	1 (0/1/0)	5 (3/2/1)	6 (2/3/1)
NTHR-NTHR	1 (0/1/0)	2 (0/2/0)	0	0	3 (0/3/0)
Total number per oligomer	5 (2/3/0)	8 (4/2/2)	13 (9/2/2)	39 (23/8/8)	65 (38/15/12)

[a] CTHR=$I^{31}IGLM^{35}$; CHC=$L^{17}VFF^{20}$ and NTHR=$V^{12}HH^{14}$. The algorithm used for the classification is explained in the structural analysis section.

analysis section). It is not only interesting to observe that the relative proportion of the different hydrophobic interactions follows the energetic ranking (in the 16 independent simulations: 20 CTHR-CHC interactions, 16 CTHR-NTHR, 10 CHC-CHC, etc.) but also that the intermonomeric distance between some hydrophobic fragments converges along the trajectory; as an example, see one of the simulations of the dimer in Figure 6. In other words, the stabilization of these interactions becomes a measure of the overall convergence and stability of these oligomers in the first step of oligomerization. Furthermore, the geometric analysis showed that the interacting strands prefers a relative orientation between 45 and 135° (perpendicular orientation) in 38 out of 65 hydrophobic contacts. Regarding the parallel or antiparallel orientation, there is no clear preference, except in the case of CTHR-CTHR and NTHR-NTHR where the antiparallel orientation is found in most cases, probably due to the effect of the terminal charged groups (-COO^- in CTHR and -NH_3^+ in NTHR). So a slight prevalence of the antiparallel over parallel orientation of the hydrophobic interacting strands is predicted, which may be related to the predominance of antiparallel β-sheets as oligomerization proceeds, as reported in several theoretical papers.[32,33,59,82] To sum up, the intermonomeric vdW steady stabilization during oligomerization can be viewed as the progressive stabilization of hydrophobic interactions in a perpendicular orientation between the three hydrophobic regions, especially CTHR-CHC intermonomeric contacts.

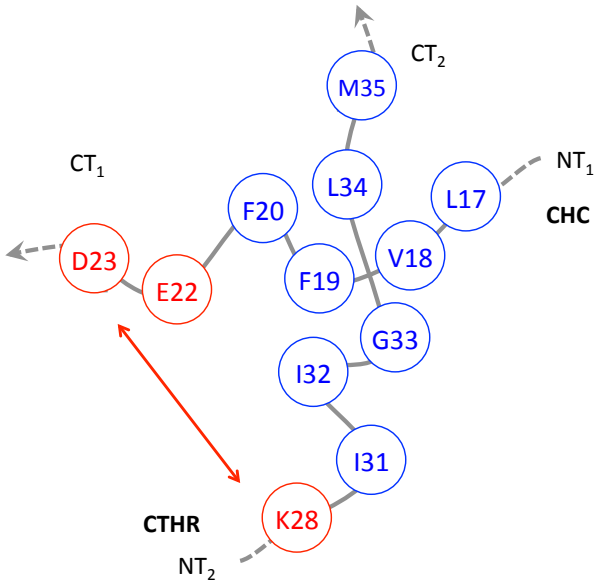

Figure 7 Residue model of the perpendicular $CTHR_2$-CHC_1 hydrophobic interaction, the substructure that favours the hydrophobic effect in the formation of early oligomers. CT and NT stand for C-terminal and N-terminal fragments, respectively. More than 50 % of the CTHR-CHC interactions (14 out of 20) adopt such a conformation whereas parallel and antiparallel orientations are less frequently observed (6 out of 20), see Table 6 and section 2.6. Apolar interactions are depicted in blue while polar interactions in red. Other secondary substructures that favour the hydrophobic effect are CTHR-NTHR, CHC-CHC and CHC-NTHR interactions, all of them mainly in pseudo-perpendicular orientation too.

The findings highlighted in the previous paragraphs show a degree of correlation with previously reported experimental and theoretical findings about the oligomerization process. Firstly, the prominent role of the CTHR fragment, which contributes to the two most favourable interaction energies, CTHR-CHC and CTHR-NTHR, could be consistent with the higher toxicity of $A\beta_{1-42}$ compared to the shorter $A\beta_{1-40}$.[74,76,103,104] Indeed, it is reasonable to think (though it is a mere hypothesis resulting from this study) that the addition of two hydrophobic residues such as I41 and A42 to the C-terminal region may foster the hydrophobic interactions between this fragment and both CHC and NTHR. Secondly, it is important to note that another important implication of the present findings is related to the binding site of Zn(II) in Aβ peptides. One of the hypotheses about the promotion of self-aggregation of Aβ peptides in the presence of Zn(II) concerns intermonomeric coordination of H13 and H14 residues in the NTHR through the metal atom,[105,106] in other words the promotion of the NTHR-NTHR interaction, which is consistent with the present model.

3.6. The secondary role of E22 and D23 residues

The hydrophobic stability that develops upon oligomerization imposes a specific conformation on the polar interactions from dimers to octamers. As seen in Figure 5 and Table S6, the residue decomposition of the total stability free energy from dimers to octamers split by intra- and inter-monomeric terms confirmed that all residues become stabilized in their intermonomeric network during oligomerization except Y10, E11, E22 and D23. The main source of stabilization for all residues corresponds to the vdW effect already explained in previous sections. However, despite the vdW stability observed for E22 and D23 of -1.6 and -1.3 kcal/mol (Figure 4 and Table S4), respectively, a total destabilization of +0.1 kcal/mol is observed for both in octamers (Figure 5 and Table S6). Additionally, the destabilization seems to be caused exclusively by intermonomeric energetic losses that are not fully compensated by the favourable intramonomeric interactions. Xu *et al.* recently studied the conformation ensemble of mutants of $A\beta_{1-42}$, reaching the important conclusion that E22 mutants create diverse alternative pathways for conformational transitions and thus increase subsequent aggregation.[107] Here, it is important to mention that E22 (E22G artic) and D23 mutants have been studied extensively due to their experimentally proven higher propensity for oligomerization, in line with the present results.[16,108]

3.7. The overall model

The combination of vdW stabilization and the reorganization of the ionic interactions during oligomer formation create a coherent overall model. Figure 7 displays the most important substructure including both apolar and polar interactions that is favoured in the oligomerization process: CTHR-CHC in perpendicular orientation. It is worth noting that this substructure promote the K28-D23/E22 interactions as

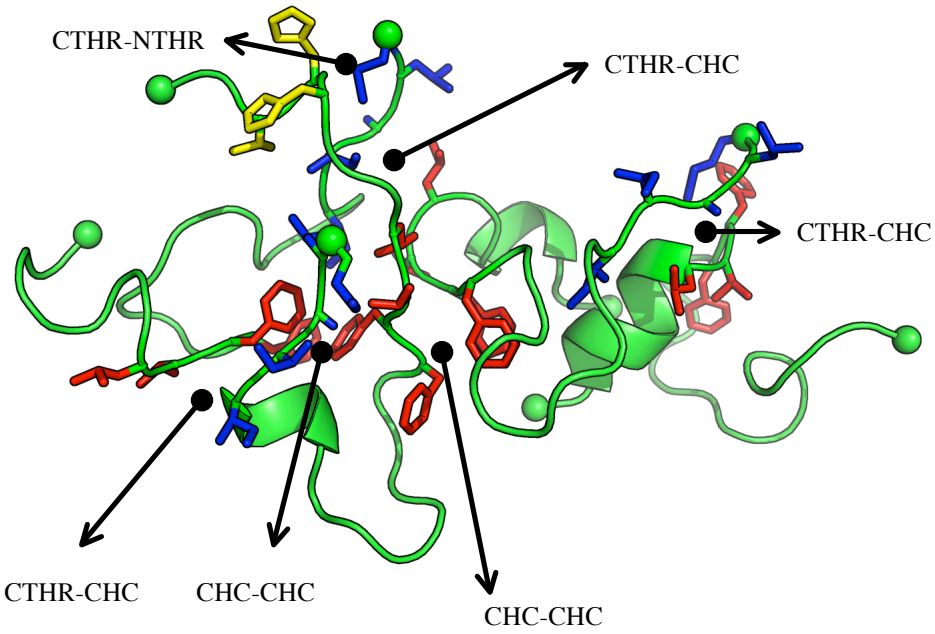

Figure 8 The centroid conformation of the most populated cluster (among 8 clusters, this cluster represents 31% of the total conformations) of the tetramer trajectories illustrating the model of oligomerization. Backbone skeleton is shown in green and residue side-chains that provide hydrophobic interactions are shown in sticks and the green balls represent N- and C-terminals. Residues in blue correspond to CTHR ($I^{31}IGLM^{35}$), residues in red form the CHC ($L^{17}VFF^{20}$) and finally residues in yellow form the NTHR ($V^{12}HH^{14}$). This structure contains six intermonomeric hydrophobic interactions (three CTHR-CHC, two CHC-CHC and one CTHR-NTHR) which exemplify the importance of these fragments in the overall stability of the oligomers.

depicted in the figure, see also Table S8 for the intermonomeric electrostatic energies of these pairwise interactions. Other secondary substructures that favour oligomerization are the hydrophobic interactions in perpendicular conformations of CTHR-NTHR, CHC-CHC and CHC-NTHR (the latter facilitates the D23/E22-K16 salt bridge formation). It is important to note that the intermonomeric polar interactions are a consequence of the hydrophobic rearrangement and not vice versa, as demonstrated by the unfavourable overall contribution of D23 and E22 to the total stability of the oligomers in the previous section. Finally, to illustrate this overall model, a molecular representation of a selected tetramer frame with some of the abovementioned interactions is displayed in Figure 8. This structure shows two CTHR-CHC, two CHC-CHC and one NTHR-CHC intermonomeric hydrophobic contacts.

4. Conclusions

Here we present the theoretical molecular basis for numerous experimental findings on the first stages of $A\beta_{10-35}$ oligomerization. We use a novel methodology involving the analysis of the MD simulations of unstructured and early-formed $A\beta_{10-35}$ oligomers (dimer, trimer, tetramer and octamer) based on the energy-type, per-residue and residue-pairwise decomposition of the MM-GBSA stability free energy. The initial dimer structures were built from the association of two monomers (PDB code 1HZ3); likewise, trimer, tetramer and octamer oligomers were initially built from the assembly of two corresponding subunits. All-atom explicit solvent MD simulations were run for four independent simulations with a total simulated time of 3.0 μs for each oligomer, except for octamers, for which the simulated time was 2.4 μs. The subsequent MM-GBSA decomposition of the stability free energy coupled to the use of multivariate data analysis techniques allowed us to unearth the most important residue-pairwise interactions that contribute significantly to the stability of these early oligomer structures. Despite the difficulty of modelling the oligomerization process we think that several significant conclusions consistent with other experimental and theoretical work can be extracted from the present study. Likewise, some findings related to residue-pairwise interactions represent a step toward the elucidation of the oligomerization process. These can be summarized as follows.

The energetic stability of all formed oligomers is clearly dominated by the apolar terms (ΔE_{vdW} and $\Delta G_{sol,apol}$), especially by the vdW term. There is a weak but steady energy stabilization as the level of aggregation increases since the octamer becomes the most stable structure as seen by the stability free energy per monomer. Furthermore, the origin of the stability that develops during oligomerization lies exclusively in the increasing stability of the intermonomeric part of the vdW term, from -30.2 kcal/mol in dimers to -59.4 kcal/mol in octamers. The combination of the two phenomena gives rise to the so-called hydrophobic effect. The per-residue and residue-pairwise decomposition also reveal that the vdW stability is caused by hydrophobic interactions between three well-defined hydrophobic fragments: 31–35 (CTHR, C-terminal hydrophobic region), 17–20 (CHC, central hydrophobic region) and 12–14 (NTHR, N-terminal hydrophobic region), ordered according to their importance. On the one hand, the CHC fragment has already been identified as a crucial element in the hydrophobic collapse and on the other

hand the prominent role of CTHR might be associated with the experimental evidence that the $A\beta_{1-42}$ peptide is more toxic than the shorter $A\beta_{1-40}$. However, further studies are required to confirm this hypothesis. Moreover, it is important to note that not all interactions among these fragments are equally important; the most prominent is the CTHR-CHC interaction followed by NTHT-CTHR, CHC-CHC and NTHR-CHC interactions in a secondary role.

The presence of hydrophobic interactions between NTHR, CHC and CTHR in the oligomers imposes a significant reorganization of the intermonomeric salt bridges. Although two complementary intermonomeric ionic interactions, K28-D23/E22 and D23/E22-K16, are favoured at expenses of other intermonomeric polar interactions, the overall role of E22 and D23 residues is unfavourable to oligomerization, which may be consistent with the experimentally higher propensity for oligomerization of the E22 and D23 mutations. For instance, the CTHR-CHC hydrophobic interaction mainly adopts a perpendicular orientation that promotes the K28-D23/E22 interaction. The combination of the hydrophobic collapse in conjunction with the reorganization of the salt bridges gives rise to an overall model similar for all oligomers that rationalizes the hydrophobic stability and the increasing stability free energy as the level of aggregation increases, especially for octamers versus smaller oligomers. The directionality (CTHR-CHC) and the main conformation (perpendicular) of the interacting hydrophobic strands are significant outcomes of the present work that will contribute to defining molecular targets for Aβ peptides.

To sum up, first, we believe that this study will stimulate theoretical and experimental studies to further confirm the directionality and the strength of the interactions between CTHR, CHC and NTHR fragments in order to facilitate the oligomerization process. And second, given the importance of soluble oligomeric Aβ forms in AD pathogenesis, it is now clear that drug design should focus on inhibitors of the oligomerization of Aβ rather than inhibitors of fibril formation. In that sense the unravelling of the factors that govern Aβ stabilization at the residue level may inspire the design of new inhibitors of the oligomerization process, which on the basis on the presented model, should be designed to interfere mainly with the hydrophobic intermonomeric interactions between CTHR and CHC hydrophobic fragments of Aβ oligomers.

Acknowledgements

We thank Prof. F. Javier Luque from our department for his valuable suggestions and comments.

Notes and references

[a] Departament de Fisicoquímica, Facultat de Farmàcia, Universitat de Barcelona, Av. Joan XXIII, s/n, Diagonal Sud, 08028, Barcelona, Catalonia, Spain. E-mail: campanera@ub.edu

† Footnotes should appear here. These might include comments relevant to but not central to the matter under discussion, limited experimental and spectral data, and crystallographic data.

Electronic Supplementary Information (ESI) available: [details of any supplementary information available should be included here]. See DOI: 10.1039/b000000x/

1. C. G. Glabe, *Neurobiol. Aging*, 2006, **27**, 570–5.
2. F. Hefti, W. F. Goure, J. Jerecic, K. S. Iverson, P. A. Walicke, and G. A. Krafft, *Trends Pharmacol. Sci.*, 2013, **34**, 261–6.
3. G. M. Shankar and D. M. Walsh, *Mol. Neurodegener.*, 2009, **4**.
4. K. A. Vossel, K. Zhang, J. Brodbeck, A. C. Daub, P. Sharma, S. Finkbeiner, B. Cui, and L. Mucke, *Science*, 2010, **330**, 198–198a.
5. D. J. Selkoe, *Nat. Med.*, 2011, **17**, 1060–1065.
6. A. S. Detoma, S. Salamekh, A. Ramamoorthy, and M. H. Lim, *Chem. Soc. Rev.*, 2012, **41**, 608–621.
7. H. W. Querfurth and F. M. LaFerla, *N. Engl. J. Med.*, 2010, **362**, 329–44.
8. H. Fukumoto, T. Tokuda, T. Kasai, N. Ishigami, H. Hidaka, M. Kondo, D. Allsop, and M. Nakagawa, *FASEB J.*, 2010, **24**, 2716–2726.
9. B. M. Austen, K. E. Paleologou, S. A. E. Ali, M. M. Qureshi, D. Allsop, and O. M. A. El-Agnaf, *Biochemistry*, 2008, **47**, 1984–1992.
10. J. P. Cleary, D. M. Walsh, J. J. Hofmeister, G. M. Shankar, M. A. Kuskowski, D. J. Selkoe, and K. H. Ashe, *Nat. Neurosci.*, 2005, **8**, 79–84.
11. S. L. Bernstein, T. Wyttenbach, A. Baumketner, J.-E. Shea, G. Bitan, D. B. Teplow, and M. T. Bowers, *J. Am. Chem. Soc.*, 2005, **127**, 2075–2084.
12. S. L. Bernstein, N. F. Dupuis, N. D. Lazo, T. Wyttenbach, M. M. Condron, G. Bitan, D. B. Teplow, J.-E. Shea, B. T. Ruotolo, C. V Robinson, and M. T. Bowers, *Nat. Chem.*, 2009, **1**, 326–331.
13. S. Lesné, M. T. Koh, L. Kotilinek, R. Kayed, C. G. Glabe, A. Yang, M. Gallagher, and K. H. Ashe, *Nature*, 2006, **440**, 352–357.
14. S. Barghorn, V. Nimmrich, A. Striebinger, C. Krantz, P. Keller, B. Janson, M. Bahr, M. Schmidt, R. S. Bitner, J. Harlan, E. Barlow, U. Ebert, and H. Hillen, *J. Neurochem.*, 2005, **95**, 834–47.
15. P. Narayan, A. Orte, R. W. Clarke, B. Bolognesi, S. Hook, K. A. Ganzinger, S. Meehan, M. R. Wilson, C. M. Dobson, and D. Klenerman, *Nat. Struct. Mol. Biol.*, 2012, **19**, 79–84.
16. I. W. Hamley, *Chem. Rev.*, 2012, **112**, 5147–5192.
17. M. R. Emmerling, *J. Biol. Chem.*, 1996, **271**, 4077–4081.
18. K. Ono, M. M. Condron, and D. B. Teplow, *Proc. Natl. Acad. Sci. U. S. A.*, 2009, **106**, 14745–14750.
19. W. H. Lin, G. D. Ciccotosto, E. Giannakis, D. J. Tew, K. Perez, C. L. Masters, R. Cappai, J. D. Wade, and K. J. Barnham, *J. Neurosci.*, 2008, **28**, 11950–11958.
20. G. M. Shankar, S. Li, T. H. Mehta, A. Garcia-Munoz, N. E. Shepardson, I. Smith, F. M. Brett, M. A. Farrell, M. J. Rowan, C. A. Lemere, C. M. Regan, D. M. Walsh, B. L. Sabatini, and D. J. Selkoe, *Nat. Med.*, 2008, **14**, 837–42.
21. M. Jin, N. Shepardson, T. Yang, G. Chen, D. Walsh, and D. J. Selkoe, *Proc. Natl. Acad. Sci. U. S. A.*, 2011, **108**, 5819–5824.
22. A. Ramamoorthy and M. H. Lim, *Biophys. J.*, 2013, **105**, 287–288.
23. B. Sarkar, V. S. Mithu, B. Chandra, A. Mandal, M. Chandrakesan, D. Bhowmik, P. K. Madhu, and S. Maiti, *Angew. Chem. Int. Ed. Engl.*, 2014, **53**, 6888–6892.
24. C. G. Glabe, *J. Biol. Chem.*, 2008, **283**, 29639–29643.
25. T. Lührs, C. Ritter, M. Adrian, D. Riek-Loher, B. Bohrmann, H. Döbeli, D. Schubert, and R. Riek, *Proc. Natl. Acad. Sci. U. S. A.*, 2005, **102**, 17342–17347.
26. R. Tycko, *Curr. Opin. Struct. Biol.*, 2004, **14**, 96–103.
27. N. W. Kelley, V. Vishal, G. A. Krafft, and V. S. Pande, *J. Chem. Phys.*, 2008, **129**, 214707.
28. S. Jang and S. Shin, *J. Phys. Chem. B*, 2008, **112**, 3479–84.
29. S. Kim, T. Takeda, and D. K. Klimov, *Biophys. J.*, 2010, **99**, 1949–1958.
30. J. Xu, J. Z. H. Zhang, and Y. Xiang, *J. Phys. Chem. A*, 2013, **117**, 6373–6379.
31. A. De Simone and P. Derreumaux, *J. Chem. Phys.*, 2010, **132**, 165103.
32. P. H. Nguyen and P. Derreumaux, *J. Phys. Chem. B*, 2013, **117**, 5831–5840.
33. F. Baftizadeh, X. Biarnes, F. Pietrucci, F. Affinito, and A. Laio, *J. Am. Chem. Soc.*, 2012, **134**, 3886–94.

34. S.-H. Chong, J. Yim, and S. Ham, *Mol. Biosyst.*, 2013, **9**, 997–1003.
35. J. A. Lemkul and D. R. Bevan, *ACS Chem. Neurosci.*, 2012, 3, 845–856.
36. P. A. Kollman, I. Massova, C. Reyes, B. Kuhn, S. Huo, L. Chong, M. Lee, T. Lee, Y. Duan, W. Wang, O. Donini, P. Cieplak, J. Srinivasan, D. A. Case, and T. E. Cheatham III., *Acc. Chem. Res.*, 2000, **33**, 889–897.
37. H. Gohlke, C. Kiel, and D. A. Case, *J. Mol. Biol.*, 2003, **330**, 891–913.
38. S. Zhang, K. Iwata, M. J. Lachenmann, J. W. Peng, S. Li, E. R. Stimson, Y.-A. Lu, A. M. Felix, J. E. Maggio, and J. P. Lee, *J. Struct. Biol.*, 2000, **130**, 130–141.
39. T. L. S. Benzinger, D. M. Gregory, T. S. Burkoth, H. Miller-Auer, D. G. Lynn, R. E. Botto, and S. C. Meredith, *Proc. Natl. Acad. Sci.*, 1998, **95**, 13407–13412.
40. O. N. Antzutkin, R. D. Leapman, J. J. Balbach, and R. Tycko, *Biochemistry*, 2002, **41**, 15436–15450.
41. J. J. Balbach, A. T. Petkova, N. A. Oyler, O. N. Antzutkin, D. J. Gordon, S. C. Meredith, and R. Tycko, *Biophys. J.*, 2002, **83**, 1205–1216.
42. R. M. Nisbet, J. Nigro, K. Breheney, J. Caine, M. K. Hattarki, and S. D. Nuttall, *Protein Eng. Des. Sel.*, 2013, **26**, 571–580.
43. G. Li and R. Pomès, *J. Phys. Chem. B*, 2013, **117**, 6603–6613.
44. K. Murakami, K. Irie, H. Ohigashi, H. Hara, M. Nagao, T. Shimizu, and T. Shirasawa, *J. Am. Chem. Soc.*, 2005, **127**, 15168–15174.
45. K. Murakami, Y. Horikoshi-Sakuraba, N. Murata, Y. Noda, Y. Masuda, N. Kinoshita, H. Hatsuta, S. Murayama, T. Shirasawa, T. Shimizu, and K. Irie, *ACS Chem. Neurosci.*, 2010, **1**, 747–56.
46. B. Ma and R. Nussinov, *Proc. Natl. Acad. Sci. U. S. A.*, 2002, **99**, 14126–14131.
47. B. Tarus, J. E. Straub, and D. Thirumalai, *J. Mol. Biol.*, 2005, 345, 1141–1156.
48. W. Han and Y.-D. Wu, *J. Am. Chem. Soc.*, 2005, **127**, 15408–16.
49. S. Jang and S. Shin, *J. Phys. Chem. B*, 2006, **110**, 1955–1958.
50. A. Kent, A. K. Jha, J. E. Fitzgerald, and K. F. Freed, *J. Phys. Chem. B*, 2008, **112**, 6175–6186.
51. G. Reddy, J. E. Straub, and D. Thirumalai, *J. Phys. Chem. B*, 2009, **113**, 1162–1172.
52. J. M. Campanera and R. Pouplana, *Molecules*, 2010, **15**, 2730–2748.
53. M. Rostkowski, M. H. Olsson, C. R. Søndergaard, and J. H. Jensen, *BMC Struct. Biol.*, 2011, **11**.
54. E. K. Gundertofte and F. S. Jorgensen, *Pharmacokinetics Molecular Modeling and Prediction of Bioavailability*, Kluwer Academic, New York, 2000.
55. High ionic concentrations induce aggregation of protofibrils. So, the Na^+ concentration was kept to a minimum as far as possible in order not to interfere with the hydrophobic effect, which is our main objective of study in this work. See, M. Gregori, V. Cassina, D. Brogioli, D. Salerno, L. De Kimpe, W. Scheper, M. Masserini, and F. Mantegazza, *Eur. Biophys. J.*, 2010, **39**, 1613–23.
56. J. Zidar and F. Merzel, *J. Phys. Chem. B*, 2011, **115**, 2075–81.
57. K. Lindorff-Larsen, S. Piana, K. Palmo, P. Maragakis, J. L. Klepeis, R. O. Dror, and D. E. Shaw, *Proteins*, 2010, **78**, 1950–1958.
58. D. Case, T. Darden, T. Cheatham, C. Simmerling, J. Wang, R. Duke, R. Luo, R. Walker, W. Zhang, K. Merz, B. Roberts, S. Hayik, A. Roitberg, G. Seabra, J. Swails, A. Goetz, I. Kolossváry, K. Wong, F. Paesani, J. Vanicek, R. Wolf, J. Liu, X. Wu, S. Brozell, T. Steinbrecher, H. Gohlke, Q. Cai, X. Ye, M. Hsieh, G. Cui, D. Roe, D. Mathews, M. Seetin, R. Salomon-Ferrer, C. Sagui, V. Babin, T. Luchko, S. Gusarov, A. Kovalenko, and P. Kollman, AMBER12, 2012, University of California, San Francisco.
59. P. H. Nguyen, M. S. Li, and P. Derreumaux, *Phys. Chem. Chem. Phys.*, 2011, **13**, 9778–9788.
60. K. R. Cho, Y. Huang, S. Yu, S. Yin, M. Plomp, S. R. Qiu, R. Lakshminarayanan, J. Moradian-Oldak, M.-S. Sy, and J. J. De Yoreo, *J. Am. Chem. Soc.*, 2011, **133**, 8586–8593.
61. D. Matthes, V. Gapsys, V. Daebel, and B. L. de Groot, *PLoS One*, 2011, **6**, e19129.
62. S.-H. Chong and S. Ham, *Phys. Chem. Chem. Phys.*, 2012, **14**, 1573–1575.
63. B. Barz, O. O. Olubiyi, and B. Strodel, *Chem. Commun. (Camb).*, 2014, **50**, 5373–5375.
64. M. Pannuzzo, D. Milardi, A. Raudino, M. Karttunen, and C. La Rosa, *Phys. Chem. Chem. Phys.*, 2013, **15**, 8940–8951.
65. L. Pan and J. C. Patterson, *PLoS One*, 2013, **8**, e70681.
66. J. M. Campanera and R. Pouplana, *Molecules*, 2010, **15**, 2730–2748.
67. B. R. Miller, T. D. McGee, J. M. Swails, N. Homeyer, H. Gohlke, and A. E. Roitberg, *J. Chem. Theory Comput.*, 2012, **8**, 3314–3321.
68. J. Seco, C. Ferrer-Costa, J. M. Campanera, R. Soliva, and X. Barril, *Proteins Struct. Funct. Bioinforma.*, 2012, **80**, 269–280.
69. W. M. Berhanu and A. E. Masunov, *J. Mol. Model.*, 2012, **18**, 891–903.
70. W. M. Berhanu and A. E. Masunov, *Biopolymers*, 2011, **95**, 573–590.
71. R Development Core team. R: A language and environment for statistical computing, R Foundation for Statistical Computing, Vienna, Austria, 2012, http://www.R-project.org.
72. B. J. Grant, A. P. C. Rodrigues, K. M. ElSawy, J. A. McCammon, and L. S. D. Caves, *Bioinformatics*, 2006, **22**, 2695–2696.
73. R. P. Joosten, T. A. H. te Beek, E. Krieger, M. L. Hekkelman, R. W. W. Hooft, R. Schneider, C. Sander, and G. Vriend, *Nucleic Acids Res.*, 2011, **39**, D411–9.
74. B. Barz and B. Urbanc, *PLoS One*, 2012, **7**, e34345.
75. M. Ahmed, J. Davis, D. Aucoin, T. Sato, S. Ahuja, S. Aimoto, J. I. Elliott, W. E. Van Nostrand, and S. O. Smith, *Nat. Struct. Mol. Biol.*, 2010, **17**, 561–567.
76. K. A. Ball, A. H. Phillips, D. E. Wemmer, and T. Head-Gordon, *Biophys. J.*, 2013, **104**, 2714–2724.
77. K. Takano, S. Endo, A. Mukaiyama, H. Chon, H. Matsumura, Y. Koga, and S. Kanaya, *FEBS J.*, 2006, **273**, 150–158.
78. V. A. Streltsov, J. N. Varghese, C. L. Masters, and S. D. Nuttall, *J. Neurosci.*, 2011, **31**, 1419–1426.
79. E. Socher, H. Sticht, and A. H. C. Horn, *ACS Chem. Neurosci.*, 2014, **5**, 161–167.
80. L. Gu, C. Liu, J. C. Stroud, S. Ngo, L. Jiang, and Z. Guo, *J. Biol. Chem.*, 2014, **289**, 27300–27313.
81. J. M. Borreguero, B. Urbanc, N. D. Lazo, S. V Buldyrev, D. B. Teplow, and H. E. Stanley, *Proc. Natl. Acad. Sci. U. S. A.*, 2005, **102**, 6015–6020.
82. B. Ma and R. Nussinov, *Proc. Natl. Acad. Sci. U. S. A.*, 2002, **99**, 14126–14131.
83. A cutoff distance of 7 Å between the mas centre of NH_3^+ and COO^- groups was used to identify this salt bridge.
84. K. A. Ball, A. H. Phillips, P. S. Nerenberg, N. L. Fawzi, D. E. Wemmer, and T. Head-Gordon, *Biochemistry*, 2011, **50**, 7612–7628.
85. W. Kim and M. H. Hecht, *Proc. Natl. Acad. Sci. U. S. A.*, 2006, **103**, 15824–15829.
86. M. Cheon, I. Chang, S. Mohanty, L. M. Luheshi, C. M. Dobson, M. Vendruscolo, and G. Favrin, *PLoS Comput. Biol.*, 2007, **3**, 1727–1738.
87. W. Hwang, S. Zhang, R. D. Kamm, and M. Karplus, *Proc. Natl. Acad. Sci. U. S. A.*, 2004, **101**, 12916–12921.
88. J. Alí-Torres, J.-D. Maréchal, L. Rodríguez-Santiago, and M. Sodupe, *J. Am. Chem. Soc.*, 2011, **133**, 15008–15014.
89. P. Faller, C. Hureau, and O. Berthoumieu, *Inorg. Chem.*, 2013, **52**, 12193–12206.
90. A. Frydman-Marom, M. Convertino, R. Pellarin, A. Lampel, R. Shaltiel-Karyo, D. Segal, A. Caflisch, D. E. Shalev, and E. Gazit, *ACS Chem. Biol.*, 2011, **6**, 1265–1276.
91. A. Frydman-Marom, R. Shaltiel-Karyo, S. Moshe, and E. Gazit, *Amyloid*, 2011, **18**, 119-127.
92. R. Cukalevski, B. Boland, B. Frohm, E. Thulin, D. Walsh, and S. Linse, *ACS Chem. Neurosci.*, 2012, **3**, 1008–1016.
93. Y. Chebaro, P. Jiang, T. Zang, Y. Mu, P. H. Nguyen, N. Mousseau, and P. Derreumaux, *J. Phys. Chem. B*, 2012, **116**, 8412–8422.
94. A. Güntert, H. Döbeli, and B. Bohrmann, *Neuroscience*, 2006, **143**, 461–475.
95. D. Meral and B. Urbanc, *J. Mol. Biol.*, 2013, **425**, 2260-2275.

96. E. A. Fradinger, B. H. Monien, B. Urbanc, A. Lomakin, M. Tan, H. Li, S. M. Spring, M. M. Condron, L. Cruz, C.-W. Xie, G. B. Benedek, and G. Bitan, *Proc. Natl. Acad. Sci. U. S. A.*, 2008, **105**, 14175–14180.
97. C. Wu, M. M. Murray, S. L. Bernstein, M. M. Condron, G. Bitan, J.-E. Shea, and M. T. Bowers, *J. Mol. Biol.*, 2009, **387**, 492–501.
98. S. Ngo and Z. Guo, *Biochem. Biophys. Res. Commun.*, 2011, **414**, 512–516.
99. B. Urbanc, M. Betnel, L. Cruz, G. Bitan, and D. B. Teplow, *J. Am. Chem. Soc.*, 2010, **132**, 4266–80.
100. D. J. Rosenman, C. R. Connors, W. Chen, C. Wang, and A. E. García, *J. Mol. Biol.*, 2013, **425**, 3338–59.
101. S. Mitternacht, I. Staneva, T. Härd, and A. Irbäck, *J. Mol. Biol.*, 2011, **410**, 357–367.
102. W. M. Tay, D. Huang, T. L. Rosenberry, and A. K. Paravastu, *J. Mol. Biol.*, 2013, **425**, 2494–2508.
103. K. N. Dahlgren, A. M. Manelli, W. B. Stine, L. K. Baker, G. A. Krafft, and M. J. LaDu, *J. Biol. Chem.*, 2002, **277**, 32046–32053.
104. Y.-S. Lin, G. R. Bowman, K. A. Beauchamp, and V. S. Pande, *Biophys. J.*, 2012, **102**, 315–324.
105. C. D. Syme and J. H. Viles, *Biochim. Biophys. Acta*, 2006, **1764**, 246–256.
106. V. Minicozzi, F. Stellato, M. Comai, M. Dalla Serra, C. Potrich, W. Meyer-Klaucke, and S. Morante, *J. Biol. Chem.*, 2008, **283**, 10784–10792.
107. L. Xu, S. Shan, and X. Wang, *J. Phys. Chem. B*, 2013, 117, 6206–6216.
108. M. M. Murray, M. G. Krone, S. L. Bernstein, A. Baumketner, M. M. Condron, N. D. Lazo, D. B. Teplow, T. Wyttenbach, J.-E. Shea, and M. T. Bowers, *J. Phys. Chem. B*, 2009, **113**, 6041–6046.
109. J. M. Campanera, X. Barril, and F. J. Luque, *Theor. Chem. Acc.*, 2013, **132**, 1–14.